Hand-held transistor based electrical and multiplexed chemical sensing system

Matti Kaisti,[*,†] Zhanna Boeva,[‡,¶] Juho Koskinen,[†] Sami Nieminen,[†] Johan Bobacka,[§] and Kalle Levon[‖]

†*University of Turku, Technology Research Center, 20014 Turun Yliopisto, Finland*

‡*Åbo Akademi University, Faculty of Science and Engineering, Laboratory of Analytical Chemistry, Biskopsgatan 8, Turku/Åbo, 20500, Finland*

¶*Lomonosov Moscow State University, Chemistry Department, Polymer Division, Leninskie gory, 1, build, 119991, Moscow, Russian Federation*

§*Åbo Akademi University, Faculty of Science and Engineering, Johan Gadolin Process Chemistry Centre, Biskopsgatan 8, Turku/Åbo, 20500, Finland*

‖*NYU Tandon School of Engineering, Department of Chemical and Biomolecular Engineering, Six Metrotech Center, Brooklyn NY 11201*

E-mail: mkaist@utu.fi

Abstract

We describe a hand-held sensing system using a transistor based multiplexed platform and a detector that couples the electrochemical information wirelessly to a smartphone. The custom disposable platform exploits the ion-sensitive FET (ISFET) technology. Via simple surface modifications the design allows a broad range of analytes to be tested with low-cost. We compared our read-out device to a commercial potentiometer using K^+ as an example species analyte. The developed sensing system has slightly better limit of detection and notably is less susceptible to external noise

which is commonly observed with potentiometers. The designed platform is fabricated using standard electronic processes with gold surface and we used commercial discrete transistors as the transducing element. It can be mass produced with high yield and low-cost. To circumvent the drift that typically occurs with modified solid state electrodes we incorporated a transducing layer between the electric conductor (gold pad) and the ionically conducting ion-selective-membrane. The polyaniline doped with dinonylnaphtalene sulfonic acid (PANI-DNNSA) was used as a transducing layer for the first time. The PANI-DNNSA layer significantly reduces the drift of the electrodes compared to a configuration without the transducing layer. The system is easy to use with a transistor based detection that can be modified for a vast variety of existing potentiometric tests.

Keywords

ISFET, solid contact, polyaniline, electrochemistry, hand-held, wireless, chemical sensing

The trend in chemical and biological sensing is towards the use of multipurpose devices that require little or no training from the user.[1,2] There are many options for the transducers converting the signal from chemical recognition into an electric signal: optical, mass, thermal and electrochemical sensors. Among the chemical sensors, the electrochemical sensors do not require external components such as bulky optical lenses or light sources and allow high level of integration and in many cases a low limit of detection. Moreover, a wide variety of off-the-shelf components are available making the electrochemical sensors especially attractive in settings where portability and low-cost are valued. These sensors are most commonly amperometric, impedimetric or potentiometric and have been successfully used as chemical and biological sensors.[1,3] From these, potentiometry provides a powerful yet simple method

for detecting several types of analytes such as nucleic acids,[4] antigens,[5,6] and trace metals.[7] The potential application areas include point-of-care diagnostics,[8] environmental monitoring,[9] food quality and safety,[10] personalized medicine[11] and more recently also wearable sensors.[12] Among the potentiometric methods the transistor based sensors provide a good alternative for disposable sensors at low-cost and robustness. If such sensors can be operated via inexpensive and simple to use measurement equipment the sensors could be utilized in a broad range of settings especially in remote and poor resource locations with minimal user training. One notable benefit can be achieved if the results can be easily shared via cloud connection allowing simple data gathering and information processing.[13] This requires a device that can access a mobile network and can make a diversity of measurements.

Several portable electrochemical systems for current based detection has been described. Rowe et al.[14] described a do-it-yourself amperometric CheapStat, but it was applicable in a laboratory setting and was designed to be a substitute for benchtop machines. A universal read-out device, uMED, was described by Nemirovski et al.[13] It was mainly developed for current based measurements, but the device also allows the measurement of commercial ion-selective-electrodes. The system, however, was limited to a single channel measurements and to measuring commercial test strips and ion-selective electrodes (ISE). A proof-of-concept for antigen detection was demonstrated using a mobile phone coupled to evalution boards and a microfluidic chip, but the system was limited to chronoamperometric measurements only.[15] Additionally, a wireless RFID smart bandage system for uric acid has been presented where the single channel read-out is achieved using amperometric detection.[16]

We set out to solve the problem of nonexisting hand held multiplexed discrete transistor based sensing system that can be used remotely anywhere and with the ability to store the numerical output to a mobile phone memory thus allowing an easy access to a mobile network. We have developed a general all electrical multiplexed sensing system (GEMSS). At the heart of the system is a disposable transistor based sensing platform coupled to a hand held readout device with a wireless data transmission to a smartphone. The sensor is

based on the ion-sensitive field-effect-transistor (ISFET) technology. ISFETs are attractive due to the small size, fast response, solid-state nature and ability to be mass produced in a standard electronic manufacturing processes with versatile post-processing abilities.

The custom platform is designed to measure two spots in the same sample simultaneously, but the technology allows far greater parallel sensing and multiplexing. The platform explicitly uses a discrete MOSFET with an extended gate structure.[17,18] This allows a low-cost solution that can be easily modified to different applications and avoids drift issues, self referencing and encapsulation issues found in CMOS based solutions[1,19–21] The FETs are biased in a low-power mode with a direct relationship between the changes in the interfacial potential and the output. The output signal is digitized and coupled to a smartphone which readily allows the connection to a mobile network and an access to cloud services and shared databases. The components of system are shown in Figure 1 A and an illustration of the sensing platforms and its operating principles in B.

Materials and Methods

Readout Device Fabrication

The electrical circuit was designed on a four layer printed-circuit-board (PCB) with skrew holes for mounting the PCB on a plastic housing. The 3D printed housing comprises three parts and allows access for changing batteries, a mechanical switch and a connector for the platform. The overall size of the system is 65 x 55 x 31 mm.

Platform Fabrication

The platform was fabricated using a PCB and standard manufacturing processes. The substrate material is the common FR4 with gold surface finish deposited with electroless nickel immersion gold (ENIG). The traces where encapsulated in the same process with liquid photoimageable solder mask. The mask was slightly extended over the pad edges.

A

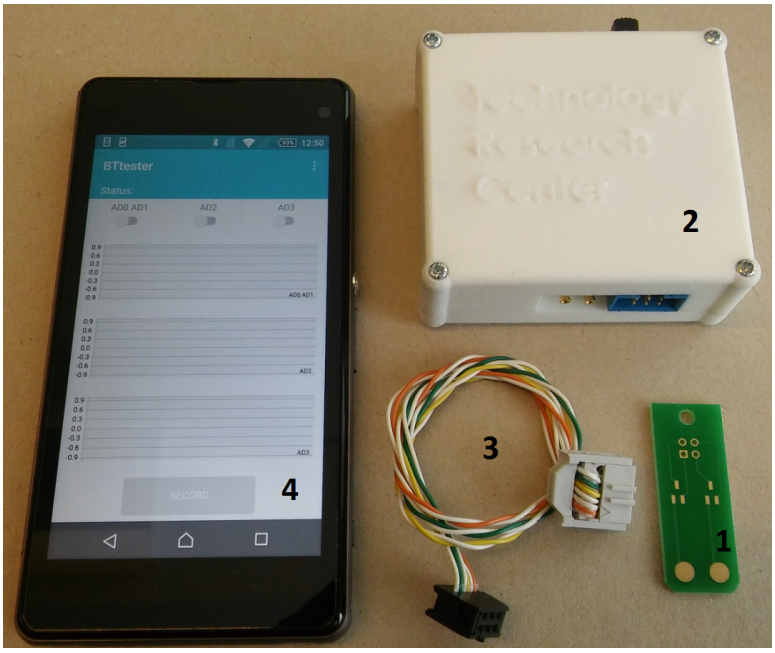

B

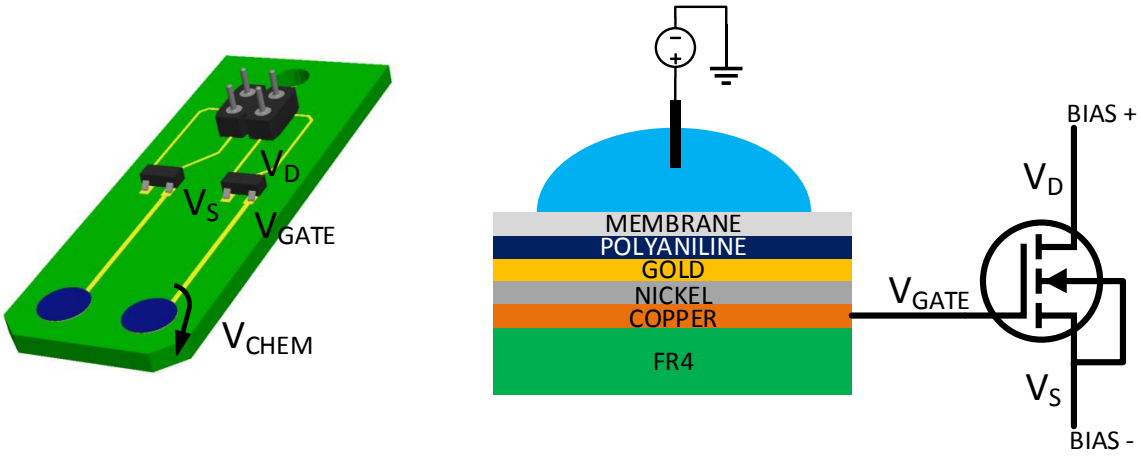

Figure 1: A) An image of the sensing system comprising; 1) the custom sensing platform; 2) the hand-held readout device; 3) cable connecting the platform to the reader and; 4) a smart phone for data plotting and storing. B) 3D image of the sensing platform (left) and a corresponding schematical illustration (right).

The commercial n-type BSS138N transistors were soldered to the platform. The transistor was chosen due to its small gate leakage current and a small input capacitance.

Chemicals

Polyaniline-dinonylnaphthalenesulfonic acid (PANI-DNNSA) was purchased from Crosslink Inc. and used without additional purification. PANI-DNNSA was dissolved in chloroform to obtain a 1.5 wt.% dispersion suitable for drop casting. Chloroform (purity >99 %) containing ethanol as a stabilizer was obtained from Sigma Aldrich.

Selectrophore® grade potassium ionophore I (Valinomycin), potassium tetrakis [3,5-bis(trifluoromethyl) phenyl] borate (KTFPB), dioctyl sebacate (DOS) and high molecular weight polyvinylchloride (PVC) were purchased from Sigma Aldrich. Tetrahydrofuran (THF) was obtained from Fluka. Sodium chloride (ReagentPlus, Sigma Aldrich) and potassium chloride (Riedel-de-Haen) were used to prepare solutions of primary and interfering ions, respectively.

Lyophilized serum, Nortrol®, Thermo, containing 3.8 mM of K^+ and 147 mM of Na^+, were recovered from lyophylizate by adding the required amount of deionized water.

Deionized water (18.2 MΩ cm, ELGA PureLab Ultra system) was used for preparation of all aqueous solutions.

Surface Functionalization

In this work three different ion-selective surface modifications of the sensing platforms where tested:

I) ISM: The ion-selective membranes were cast directly onto the gold pad.

II) PANI-DNNSA | ISM: PANI-DNNSA was used as a transducing layer between the gold surface and the ion-selective-membrane.

III) PANI-DNNSA(EtOH) | ISM: Same as (II), but PANI-DNNSA was treated with ethanol prior to ion-selective membrane casting.

When polyaniline was used as transducing layer (II and III) it was deposited by drop casting 8 μL of PANI-DNNSA solution (1.5 wt.% dispersion in chloroform) onto each sensing

pad and left drying overnight. The (III) platforms were placed in 70% ethanol for 1 minute to remove the excess of DNNSA and improve the electroactivity of the material.[22]

The K^+-selective membrane was prepared by dissolving 1.57 mg of potassium ionophore I, 0.78 mg of KTFPB, 102.29 mg of DOS and 52.24 mg of PVC in 1 mL of THF. The obtained solution was shaken briefly using a vortex mixer and left on a nutation platform overnight to ensure dissolution of PVC. The platforms were cast with 17.2 μL of the K^+-selective membrane solution and left drying overnight.

Measurement Equipment

Open-circuit-potentiometric (OCP) measurements were carried out in a two-electrode cell. For OCP measurements simple wires were soldered to the platform without the transistors and the wires were connected to a commercial 16-channel high impedance (10^{15} Ω) voltmeter (Lawson Lab Inc., Malvern, PA). A conventional Ag|AgCl|3 M KCl reference electrode was used in all measurements. When the calibration curves where obtained, the potentials were corrected with the liquid junction potentials using the Henderson equation and the activity coefficients were calculated using the Davies equation.

Electrical Transducer

ISFET Fundamentals

The designed extended-gate FET (EGFET) structure operates under the same principle as ISFETs fabricated in the unmodified CMOS processes. The gate of the MOSFET is not removed but extended to a sensing layer via conductive wire. Thus the MOSFET threshold voltage V_{th}^{mosfet} remains as such and additional contributions from the chemical part need to be added to describe the ISFET threshold voltage[23]

$$V_{th}^{isfet} = V_{th}^{mosfet} + V_{cell} \tag{1}$$

An electrochemical cell has several phases and interfaces and across each of them there is a potential difference. The potential of the entire electrochemical cell is a sum of these potentials.[2] The cell consisting of an ion-selective-electrode, sample solution and the reference electrode (REF) has several constant interfacial potentials and they can be lumped into a single constant called the standard potential V_{cell}^{0} and the cell potential can be expressed with the Nikolsky-Eisenman equation

$$V_{cell} = V_{cell}^{0} + \frac{RT}{z_i F} \ln(a_i + K_{i,j} a_j^{z_i/z_j} + L) \tag{2}$$

where a is the activity (i for the primary ion and j for the interfering ion), $K_{i,j}$ is the selectivity coefficient, L is included for the limit of detection and z is the valence of a spesific ion. R,T and F are the gas constant, temperature and the Faraday constant respectively. This extended version of the Nernst equation allows the estimation of the sensors selectivity and detection limit when the parameters $K_{i,j}$ and L are extracted experimentally.[24] As implied by Equation 1 the electrochemical cell potential is modified by the V_{th}^{mosfet}; an electrical component placed in series with the other components of the cell. In a typical case the transistor threshold voltage is the dominant component in the ISFET threshold voltage V_{th}^{ISFET} which is the amount of voltage needed to apply to the REF to turn on the device. The membrane potential being the only variable of the system a simple relation between the change in V_{th}^{isfet} ISFET (with n-type MOSFET) and a change in the V_{cell} reads

$$\Delta V_{cell} = -\Delta V_{th}^{isfet} \tag{3}$$

Furthermore, the electrical bias circuit can be designed in a way that the chemically induced potential changes at the transistor gate are directly related to potential changes at the source node.

Custom ISFET Platform

We developed an ISFET platform by combining discrete MOSFETs to a custom PCB. The gate of the MOSFET was extended via the PCB's gold trace to a circular pad with 4 mm diameter. The diameter can be reduced in size if a smaller size or higher pad density in highly multiplexed applications is required. The pad extension from the transistor is substantial enough to allow simple immersion of the pads into a solution while leaving the transistors in air. This eliminates any transistor encapsulation problems. The sensitivity towards a chemical target is achieved by using an ion-sensitive membrane. This is complemented by an organic polymer deposited on the gold pad as an intermediate ion-to-electron transducer.[24] This transducing layer ensures robust and reliable sensor performance by acting as a mediator between the ionic and electric conductors.[25,26] Conducting polymers are efficient mediators because they are both electrically and ionically conductive when doped. This allows the transduction of the ionic signal at the membrane interface into an electronic signal. The polymer layer creates a large interfacial redox capacitance and stabilizes the sensing system against disturbances. Two pads were implemented in a single platform that can be measured simultaneously. The platform can be manufactured fully in a commercial manufacturing processes. We have described a platform with the same basic principle earlier.[18]

Design of the Universal Detector

Figure 2 A) shows the block diagram of the device. It includes (i) a two channel analog-front-end that utilizes a constant-voltage-constant-current (CVCC) bias circuitry which ensures direct relation with between changes at the sensing layer voltage and output and is constructed with op-amps (LTC6079 Linear) and passive components as depicted in Figure 3); (ii) a four channel 16-bit ADC (ADS1115 TI) which measures the output of two sensors and (iii) the voltage from temperature measuring circuit implemented as voltage divider where a PT1000 sensor element is placed at the custom sensor platform and it has an uncertainty of $\pm$ 0.3 K including the element and the biasing and readout circuit; (iv) single channel

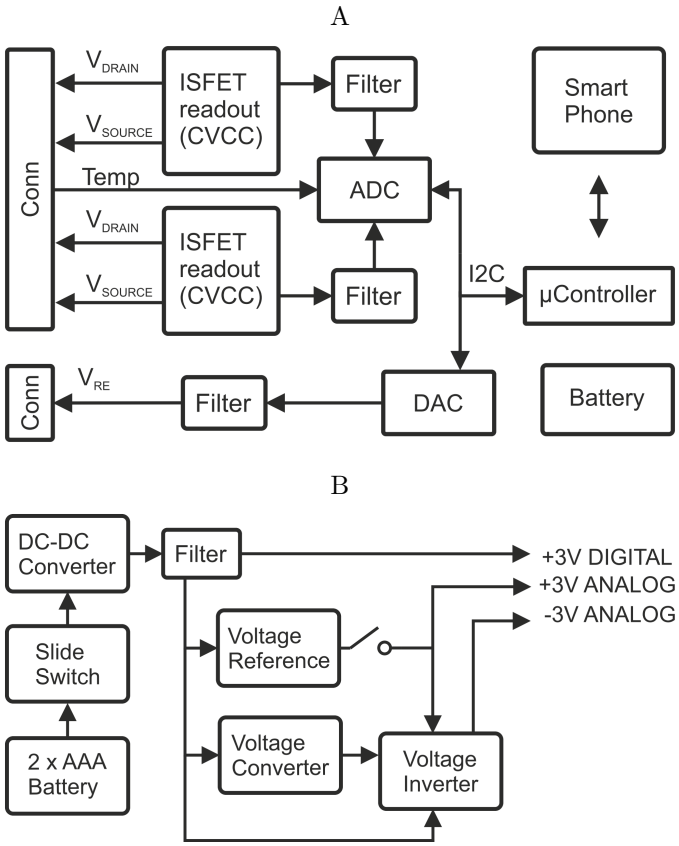

Figure 2: A) Block diagram of the read-out device. B) Power generation for the read-out device from battery.

16-bit DAC (MCP4725 Microchip) that provides bias to the reference electrode; (v) DC-DC converter (TPS61220 TI) that keeps the voltage from the pair of AAA batteries constant (vi) low noise voltage reference (LM4120-3.00 TI) for a bias circuit that drive the sensors for precision analog signal measurements (vii) voltage converter (TL7660 TI) that inverts a positive signal to a negative signal coupled with (viii) op-amp inverter (LTC2054 Linear) that draws negative supply from the noisy converter signal and inverts the stable positive reference signal; (ix) analog switch (TS3A4741 TI) that is used to couple/decouple the analog-front-end (AFE) and ;(x) microcontroller unit (RFD22301 RF Digital) that controls the data acquisition and transmission to a smartphone using a low energy Bluetooth.

Figure 2 B) shows the block diagram of the power generation. A mechanical slide switch is used to decouple the batteries from the electronics to avoid any leakage current during stand by. The digital and analog power domains are separated to make sure that the digital switching noise does not weaken the noise properties of the biasing circuit. A positive voltage reference provides a low noise voltage source for the CVCC. From the same positive reference also the negative reference is generated by a simple op-amp inverter. The inverter draws negative supply voltage from a noisy negative potential converter, but inverts a stable positive reference. The inverting op-amp is selected for low power and high power supply rejection ratio. Such a configuration allows the source node to swing to negative potential, a requirement if one chooses to ground the reference electrode for a simpler configuration.

Analog Front-End

The analog-front-end (AFE) consists of bias circuitry, analog-to-digital converter (ADC), digital-to-analog conventer (DAC) and an analog switch. The bias for transistors is implemented by a CVCC circuit and shown in Figure 3 with a connection to the sensing platform. The voltage across the MOSFET is fixed at 1.2 V and both current sources are fixed for 120 μA operation (either source or sink). This configuration leads to a constant voltage and a constant current operation. Both the MOSFET drain voltage (V_D) and source volt-

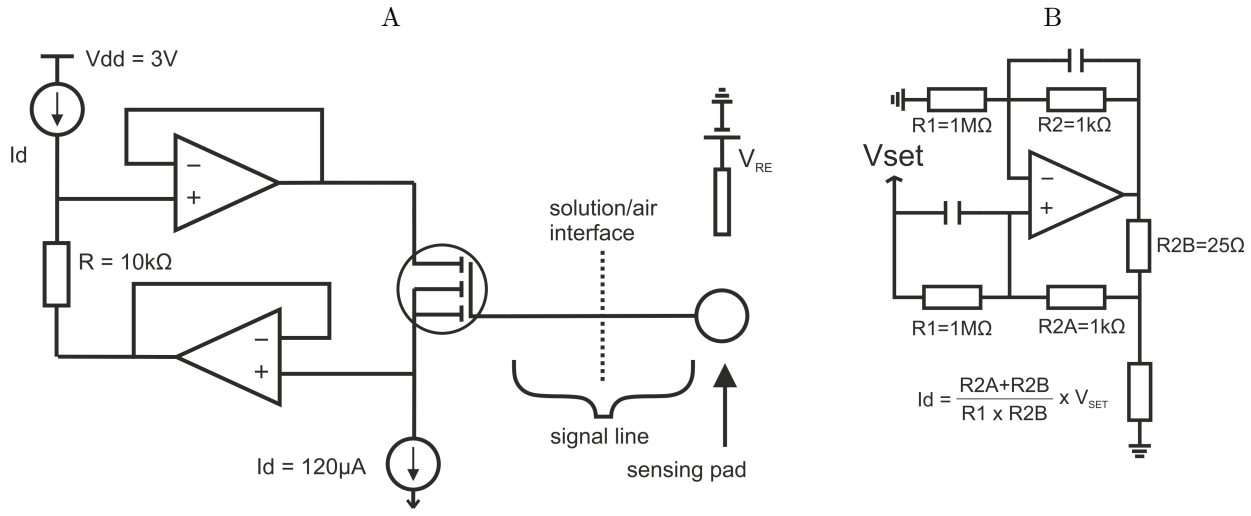

Figure 3: A) Circuit presentation of the custom platform coupled to the bias circuitry. B) Current generator used in the bias circuits for both current sourcing and sinking.

age (V_S) shift according to changes at the MOSFET gate (V_G) allowing the gate-to-source (V_{GS}) remain constant as required by the constant I_D and constant V_{DS}. Measuring the buffered V_S of the MOSFET (with respect to ground) the interfacial potential changes are obtained in linear relation i.e. ΔV_S equals ΔV_{chem}. ADC is used to digitize the V_S of both channels as well as the temperature sensor reading. The DAC provides a stable potential for the reference electrode that sets the bulk solution potential. The analog switch is used to protect the bias circuitry and transistors when the platform is not connected to the input. The switch decouples the bias circuit by turning off both the negative and positive power sources.

User Interface

A custom Android application was developed for establishing a connection to the μController, plot measured data on the phone screen in real-time and for storing the data to the phone memory. The flow chart describing the software operation is shown in Figure 4. The phone connects and communicates wirelessly with the μController with a low energy Bluetooth (BLE). A BLE service scans and connects the phone to the μController and handles the

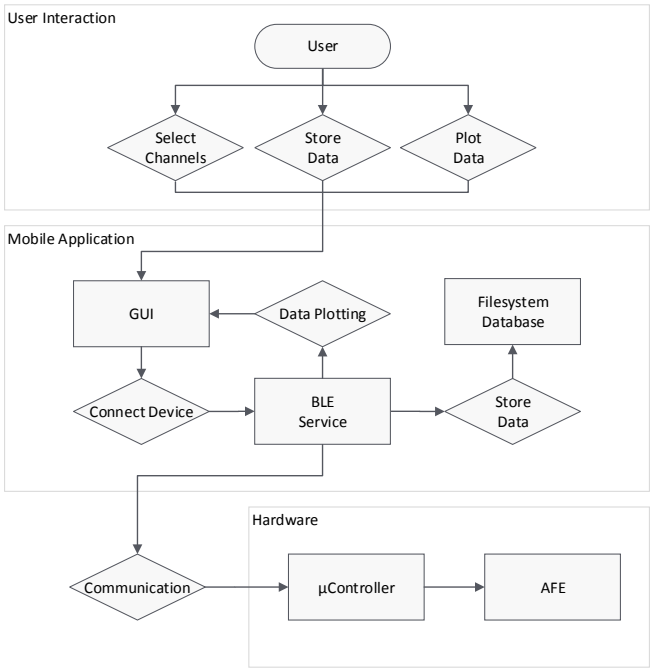

Figure 4: A flow chart depicting the user interface and the operation of the GEMSS which allows phone initiated detection with data plotting and storage.

data transmission. The user starts the scan from the application's home screen and the application automatically scans and connects to the correct μController and proceeds to displaying data to the user. On the data view the user can select which channels to plot. Once a channel is selected the application sends a message to the μController to start sending data. After the transmission is enabled the data can be recorded and stored directly to the phone's filesystem.

The Android application uses a model view controller (MVC) design pattern. A fragment class working as a controller coordinates commands between the user interface (View) and the Model (BLE service and Filesystem). The flow proceeds as follows: when the user initiates a scan the fragment starts a BLE service. The BLE service sends information such as device found or the measured data back to the fragment. If a user has chosen to plot the data the fragment then modifies the View accordingly and if data storage is chosen the fragment stores data with the help of the Filesystem Database. The fragment listens to the BLE service and the View continuously.

Embedded Software

The μController handles communication between the AFE and the Android application and it is designed to keep the amount of wirelessly transmitted data minimal. The embedded software is controlled with commands sent by the Android application via Bluetooth. These commands define which of the preset operating modes is used. The controller communicates using the I2C with the analog switch, ADC and DAC which together comprise the AFE and sets their operation depending on which channels are selected for monitoring. When the system is not recording the bias circuitry is decoupled from the rest of the electronics. Depending on which channel is measured the ADC is configured accordingly and the bias is turned on as well as the DAC. The DAC voltage is set to 2.1V. This provides an output baseline around 1V as the sensor threshold voltage is subtracted from the applied bias voltage in the measuring circuit. The sampling rate for each selected channel is 10 Hz in the μController before the data is propagated to the phone with a timestamp.

Results

Device Performance

The linearity of the AFE was tested by correlating a ramp signal fed directly to FET gates and the output of the CVCC circuit. This is shown in Figure 5. The AFE provides a linear relationship between the transistor gate and the measured output. The overall current consumption of the GEMSS from 3V battery is slightly less than 6 mA with 10 Hz sample frequency with the wireless data transmission on. The system uses a mechanical switch that fully decouples the batteries from the electronics allowing the full battery capacity to be used even with long intervals between the measurements. The battery life of the device is about 300 h when measuring and the data transmission is on.

Although the device operates at a low power it provides the same performance as com-

mercial devices. In Figure 7 C) the reader performance is compared using the same EGFET platforms in ISFET and OCP configurations. The dectection limit is systematically observed to be slightly better with the ISFET configuration using GEMSS.

The sensitivities are practically identical. The comparison is done with and without interfering 0.1 M NaCl. The EGFET configuration is practically noise-free from external disturbances as the impedance conversion from high to low takes place physically near the chemical reaction.

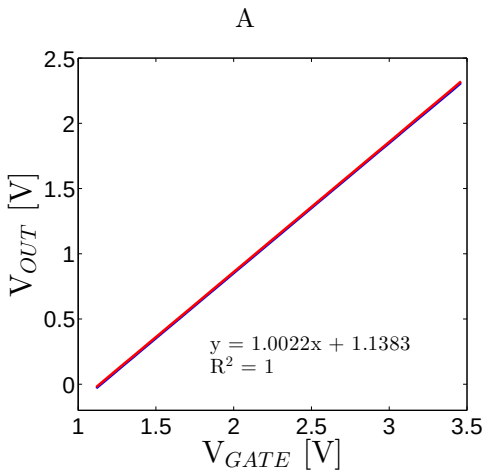

Figure 5: Linearity of the analog-front-end. The input signal is swept from about 1 V to 3.5 V and connected directly to the transistor gate. The two channels measured simultaneously show almost completely overlapping responses indicate very small difference between the transistor threshold voltages.

Comparison of the Modified Platforms

The drift of the sensing platforms were monitored by comparing all three different modification alternatives by placing them in a 0.1 M KCl solution. Typical time evolutions of the platforms are shown in Figure 6 A for OCP configuration and Figure 6 C for the ISFET. Recording of the potentials was started immediately after the electrodes were brought in contact with the primary ion solution for the first time, i.e. without any pre-conditioning of the electrodes. The platforms with PANI-DNNSA as a solid contact reach equilibrium potential and stable operation substantially faster than the platforms without the polyaniline

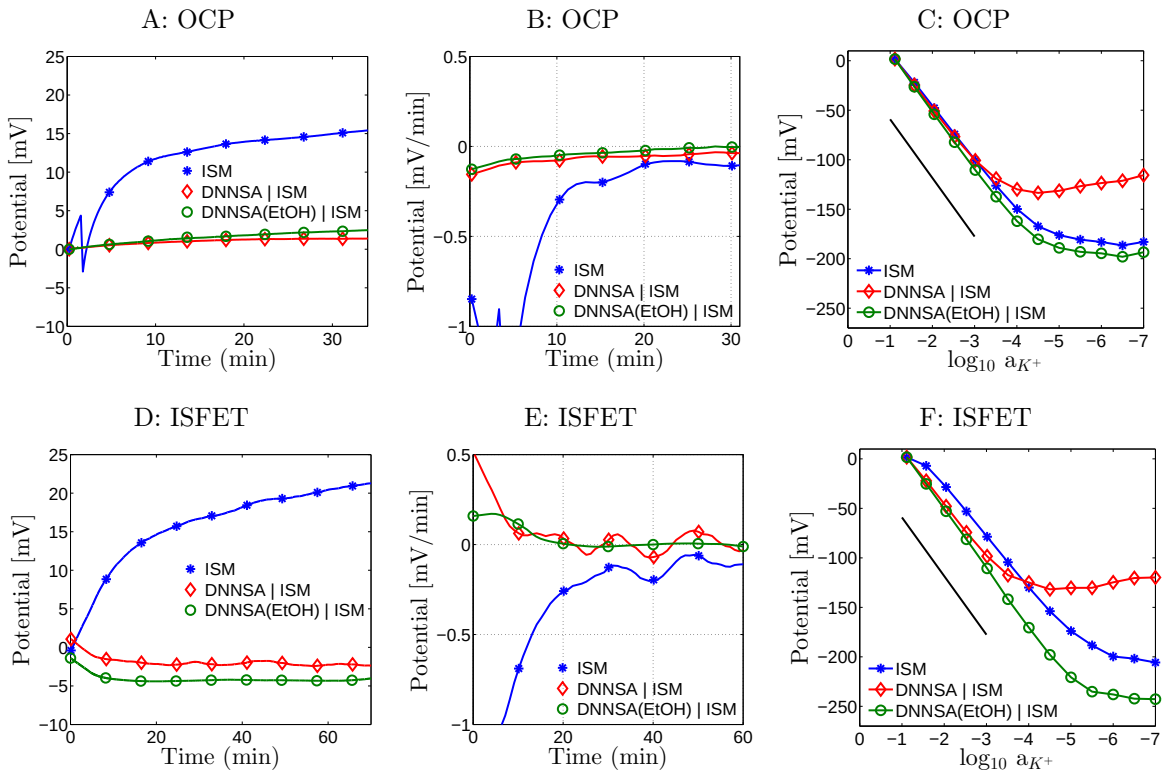

Figure 6: Different membrane composition comparisons by measuring the platforms in OCP and ISFET configurations. All measurement were done in KCl solutions. The drift was measured in 0.1 M KCl and the calibration curves were obtained by half decade step dilutions starting from 0.1 M KCl. A) OCP time evolution B) OCP drift as mV/min C) OCP calibration D) ISFET time evolution E) ISFET drift as mV/min F) ISFET calibration. In B) and E) the plotted drift values are extracted by computing the potential difference of subsequent 1 min time bins.

layer. The ISM configuration (I) do not exhibit stable operation. Although configuration (I) occasionally showed non-drifting operation the results are non-reproducible. Both configurations with polyaniline (II and III) show significantly improved stability. The stability is further explored by dividing the time evolution measurements into 1 min bins and computing the potential difference of these bins. This reveals the drift values in mV/min for the entire recording time and are plotted in Figure 6 B and E. In both cases the configuration (I) shows over 1 mV/min drift after-which it starts to stabilize, but never reaches a stable operation. The configuration (II) shows clearly better stability for ISFET and OCP. However, ISFET demonstrates instability in shorter time scale and in OCP there is a slight upward drift. As

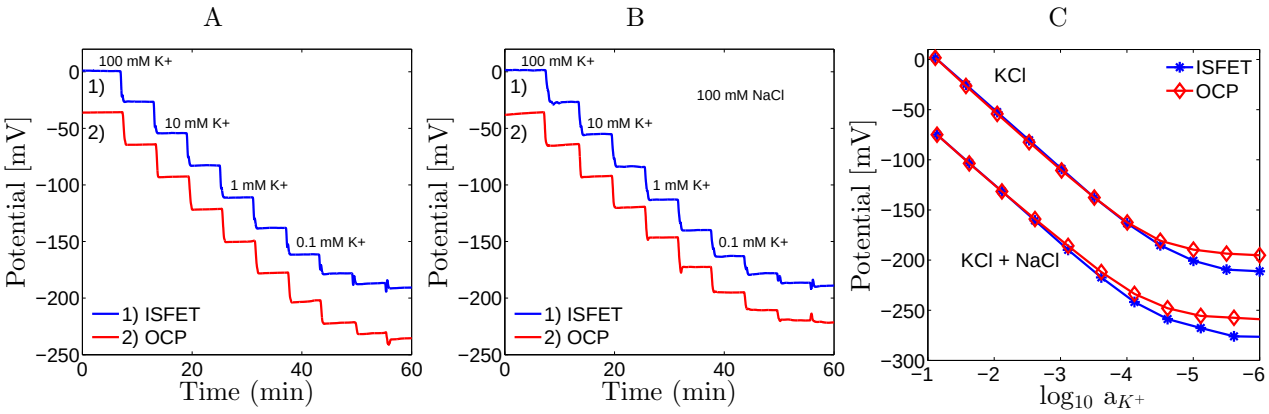

Figure 7: Trace calibration curves for both OCP and ISFET configuration with B) and without interfering ions A) and end point calibration curves collected in C with average of four measurements for each case.

indicated by A and D, the configuration (III) shows very good stability and in the ISFET case, the drift is practically unnoticeable.

If the membrane is directly casted onto the surface of the gold pad the conversion of ion signal, generated by the difference of chemical potentials between analyte|membrane and membrane|metal interfaces, occurs through the charging of the double layer of the metal. The capacitance of this double layer is very small and therefore every small change in the system causes a large change in the recorded potential. Using conducting polymers as intermediate layers with high redox capacitance provide a reversible ion-to-electron transduction via the redox reactions of the polyaniline using the target ion and/or its hydrophobic counterion. We used PANI-DNNSA, where DNSSA is a bulky counterion. When PANI-DNNSA was not treated with ethanol there is an excess of DNNSA in the solid contact that is soluble in the membrane cocktail and migrates into the membrane. This changes the electro-neutrality of the membrane and disrupts its functionality. When the PANI-DNNSA is treated with ethanol, the excess of DNNSA is removed and the solid contact becomes insoluble. This keeps the solid contact intact and provides the best possible conversion of ionic signal into electronic signal. The washing of the excess of DNNSA also improves the electroactivity of the material[22] and we assume that this improves the signal transduction properties as well.

Calibration curves of each configuration, however, reveal that configuration II has much smaller dynamic range compared to the I and III. Both OCP and ISFET configuration show similar responses as shown in Figure 6 B and D. We assume that the reduced dynamic range of II is caused by the solubility of the upper part of the solid contact which dissolves into the ISM. We additionally attribute the difference in the configuration (II) stabilities between OCP and ISFET to a difference in the membranes, probably arising from a different degree of dissolving of the solid contact into the ISM. The platforms with PANI-DNNSA(EtOH) exhibit similar dynamic range as I but with higher potential stability and therefore configuration III was chosen for further studies.

Figure 7 A and B represent potential-time calibration curves for composition III. The electrodes demonstrate a good potential stability throughout the entire concentration range of the titration and each dilution step is accompanied with a sharp stepwise decrease of the potential and a short equilibration time. The electrodes show no drift, which is typical for ion-selective electrodes having relatively hydrophobic solid contacts.[27,28] The platforms were additionally calibrated in the presence of 0.1 M NaCl. The test provides information of the electrode behavior in the presence of an interfering ion. Figure 7 A and B show the potential-time calibration curves for both OCP and ISFET configurations. The interferent (Na^+) can interact with the ISM when the concentration difference to the primary ion is several orders of magnitude higher (selectivity coefficient for the membrane is log $K_{K,Na}$ = -4.1). However, the electrodes show similar limit of detection in the presence of interfering ions and good stability with a short response time.

To evaluate the slope and limit of detection of the electrodes the potential-time calibration curves were processed to end point calibration plots presented in Figure 7 C. Both OCP and ISFET configurations show near Nernstian response with linear dynamic range with four orders of magnitude. An average of four calibration curves for each case is shown. The limit of detection and the sensitivity values are collected in Table 1.

Table 1: The limit of detection (L) (as defined by IUPAC[29]) extracted for both ISFET and OCP configurations under KCl and KCl + NaCl solutions. The KCl initial condition is 0.1 M ($\log_{10}$ a_K^+ = -1) and NaCl is kept at 0.1 M.

	L ($\log_{10}$ a_K^+)		Slope (mV/dec)	
	ISFET	OCP	ISFET	OCP
KCl	-4.8	-4.5	-58.2 ± 0.9	-58.2 ± 0.2
KCl + NaCl	-4.7	-4.4	-59.4 ± 0.6	-57.1 ± 0.6

Blood Serum Measurement

The applicability of the low-cost disposable platforms for POC analysis was tested by measuring potassium ions in blood serum. The purpose of the blood serum analysis test was to investigate the performance of the developed sensor under one of the most demanding tests for ISE and is used here as an example of a real application. With sequential dilutions of the recovered blood serum sample we studied the response of the GEMSS with configuration III. Figure 8 shows a typical time evolution of the electrode potential when diluted with deionized water (2-fold dilutions). The electrodes provide fairly stable potential. However, the drift is clearly higher in serum than in solutions containing primary ions only as shown in Figure 8 A). The calibration curve (Figure 8 B) shows the mean and standard deviation of four measurements. The response is slightly sub-Nernstian. The observed deviations and drift are typically caused by the complex matrix of the sample, i.e. presence of proteins and other metal ions, such as Ca^{2+} and Mg^{2+} in high concentration that limit the performance of the electrodes in real samples.[30]

We used the standard additions method to determine the concentration of potassium ions in a diluted serum sample.[31] The method allows detecting the concentration of an analyte in a complex matrix by simply adding a known amount of the detectable ions into the analyte. The used method requires that the slope of the sensor is known. The average slope of the calibration curve obtained from the Figure 8 B) was found to be 44 mV/dec. This slope was used in the standard additions method as a fixed slope. This simplifies the user experience as the slope can be determined prior to the actual measurement. We expect this simplification

to reduce the precision of the measurement as the slope can not be expected to be exactly the same between the sensors. The reason for the sub-Nernstian sensitivity (slope) in serum is presently unknown and would deserve a further study, especially if the sensor would be intended for clinical analysis.

The serum sample has a known K^+ concentration of 3.8 mM and after 16 fold dilution the concentration is 0.238 mM. The diluted samples where spiked three times with known concentrations of K^+ in water. This was repeated for three individual sensors. For each standard addition the K^+ concentration can be computed if the slope of the sensor is known. This revealed that the measured K^+ concentrations (averages over the three values obtained by spiking the sample three times) for three individual sensor measurements are : (0.25 ± 0.07), (0.18 ± 0.03) and (0.26 ± 0.04) in units of mM. It is expected that the deviations in the measurements follow the normal distributions with zero mean and thus by increasing the amount of parallel measurements of the same reaction we expect that the accuracy can be increased by simple averaging. Considering the average of the three measurements we obtained a value 0.230 mM (3.68 mM) which is fairly close to the expected value of 0.238 mM (3.80 mM) for the commercial serum sample.

The blood serum measurements demonstrate the potential application of the developed platform in POC although the precision is not sufficient for strictly clinical use. The electrodes are not exempt of a fundamental problem of the irreproducibility of the standard potential and specific protocols have to be employed[30] for real clinical applications. In the future, the accuracy can be improved by adjusting the solid contact composition, precise dilutions of the serum sample and by using automated systems for depositing the ISM and the solid contact onto the sensing pads as well as improving the calibration method.

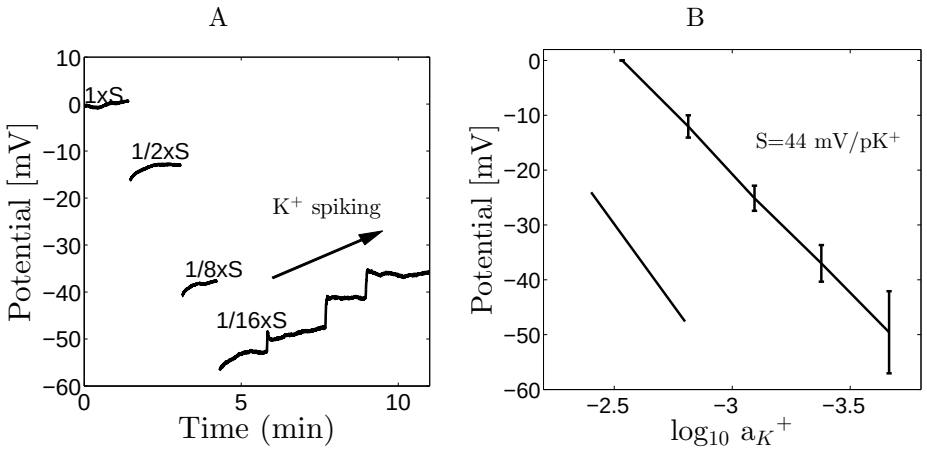

Figure 8: GEMSS used for blood serum measurements. A) Trace calibration curve for serum dilution. B) End point calibration with four measurements.

Discussion

The GEMSS relies on commercial electrical components and manufacturing processes. The disposable platform comprises of a common electrical printed-circuit-board with commercial transistors. The cost of the disposable platform is around 0.3 eur quoted for 1000 units. This, however, excludes the cost of depositing chemically reactive materials to the surface which provides the cost bottleneck for the platform. The reader was not cost optimized, but a similar design could be pushed well below 100 eur excluding the phone.

We have shown the robustness of the system via ion-selective electrodes with comparable performance to benchtop devices that use more bulky and expensive electrodes. The used conducting polymers additionally allow further expansion of the system towards enzymatic reactions and antibody/antigen interactions[6] or DNA detection.[4] The platform, however, is not limited to conducting polymer based reactions and the gold surface could be directly functionalized with oligonucleotide probes or proteins (antigens or antibodies), or modified with mediator layers such as graphene.

The versatility of the system stems from the use of commercial components and manufacturing systems coupled with the digital domain. The Arduino based microcontroller environment allows very simple possibilities for reprogramming and modifications. The

drawback of such controllers is the cost, but practically any microcontroller can be used. The accurate and standalone DAC allows arbitary waveform generation that could allow enhanced detection via field-effect modulation[32–34]

Conclusions

We demonstrated a generic electrical multiplexed sensing system (GEMSS) for charge based non-Faradaic sensing. Our approach uses commercial components and manufacturing processes. The designed platform allows a wide variety of different chemical sensing layers to be deposited making the system highly versatile. It was found that when the system is applied for ion sensing the disposable electrode has a low initial drift and thus requires minimal conditioning prior to use making it suitable as an in-situ ion selective electrode. The detection is fully automated and requires minimal user training. The data is automatically sent wirelessly to a smartphone where the data is stored and if required post-processed and shared via mobile networks. The developed system provides a step towards hand-held potentiometric sensing with capabilities broadly in the (bio)chemical world.

References

(1) Janata, J. *Principles of Chemical Sensors*, 2nd ed.; Springer Publishing Company, Incorporated, 2009.

(2) Vanamo, U. Solid-State Reference and Ion-Selective Electrodes - Towards Portable Potentiometric Sensing. Ph.D. thesis, Åbo Academi, 2013.

(3) Ronkainen, N. J.; Halsall, H. B.; Heineman, W. R. Electrochemical biosensors. *Chem. Soc. Rev.* **2010**, *39*, 1747–1763.

(4) Goda, T.; Singi, A. B.; Maeda, Y.; Matsumoto, A.; Torimura, M.; Aoki, H.; Miya-

hara, Y. Label-Free Potentiometry for Detecting DNA Hybridization Using Peptide Nucleic Acid and DNA Probes. *Sensors* **2013**, *13*, 2267.

(5) Figueiredo, A.; Vieira, N.; Santos, J. D.; Janegitz, B. C.; Aoki, S.; Peitl, P.; Lovato, R.; Nogueira, M.; Zucolotto, V.; Guimara, F. Electrical Detection of Dengue Biomarker Using Egg Yolk Immunoglobulin as the Biological Recognition Element. *Scientific Reports* **2015**, *5*, 7865.

(6) Zhang, Q.; Prabhu, A.; San, A.; Al-Sharab, J. F.; Levon, K. A polyaniline based ultrasensitive potentiometric immunosensor for cardiac troponin complex detection. *Biosensors and Bioelectronics* **2015**, *72*, 100 – 106.

(7) DeMarco, R.; Clarke, G.; Pejcic, B. Ion-Selective Electrode Potentiometry in Environmental Analysis. *Electroanalysis* **2007**, *19*, 1987–2001.

(8) Gubala, V.; Harris, L. F.; Ricco, A. J.; Tan, M. X.; Williams, D. E. Point of Care Diagnostics: Status and Future. *Analytical Chemistry* **2012**, *84*, 487–515.

(9) Mimendia, A.; Gutierrez, J.; Leija, L.; Hernandez, P.; Favari, L.; Munoz, R.; del Valle, M. A review of the use of the potentiometric electronic tongue in the monitoring of environmental systems. *Environmental Modelling and Software* **2010**, *25*, 1023 – 1030, Thematic issue on Sensors and the Environment - Modelling and ICT challenges.

(10) Ciosek, P.; Wroblewski, W. Potentiometric Electronic Tongues for Foodstuff and Biosample Recognition - An Overview. *Sensors* **2011**, *11*, 4688.

(11) Kahn, J. G.; Yang, J. S.; Kahn, J. S. Mobile Health Needs And Opportunities In Developing Countries. *Health Affairs* **2010**, *29*, 252–258.

(12) Gao, N.; Zhou, W.; Jiang, X.; Hong, G.; Fu, T.-M.; Lieber, C. M. General Strategy for Biodetection in High Ionic Strength Solutions Using Transistor-Based Nanoelectronic Sensors. *Nano Letters* **2015**, *15*, 2143–2148.

(13) Nemiroski, A.; Christodouleas, D. C.; Hennek, J. W.; Kumar, A. A.; Maxwell, E. J.; Fernandez-Abedul, M. T.; Whitesides, G. M. Universal mobile electrochemical detector designed for use in resource-limited applications. *Proceedings of the National Academy of Sciences* **2014**, *111*, 11984–11989.

(14) Rowe, A. A.; Bonham, A. J.; White, R. J.; Zimmer, M. P.; Yadgar, R. J.; Hobza, T. M.; Honea, J. W.; Ben-Yaacov, I.; Plaxco, K. W. CheapStat: An Open-Source, Do-It-Yourself, Potentiostat for Analytical and Educational Applications. *PLoS ONE* **2011**, *6*, 1–7.

(15) Lillehoj, P. B.; Huang, M.-C.; Truong, N.; Ho, C.-M. Rapid electrochemical detection on a mobile phone. *Lab Chip* **2013**, *13*, 2950–2955.

(16) Kassal, P.; Kim, J.; Kumar, R.; de Araujo, W. R.; Steinberg, I. M.; Steinberg, M. D.; Wang, J. Smart bandage with wireless connectivity for uric acid biosensing as an indicator of wound status. *Electrochemistry Communications* **2015**, *56*, 6 – 10.

(17) Prodromakis, T.; Liu, Y.; Toumazou, C. A Low-Cost Disposable Chemical Sensing Platform Based on Discrete Components. *IEEE Electron Device Letters* **2011**, *32*, 417–419.

(18) Kaisti, M.; Knuutila, A.; Boeva, Z.; Kvarnström, C.; Levon, K. Low-Cost Chemical Sensing Platform With Organic Polymer Functionalization. *IEEE Electron Device Letters* **2015**, *36*, 844–846.

(19) Janata, J. Graphene Bio-Field-Effect Transistor Myth. *ECS Solid State Letters* **2012**, *1*, M29–M31.

(20) Hu, Y.; Georgiou, P. A Robust ISFET pH-Measuring Front-End for Chemical Reaction Monitoring. *IEEE Transactions on Biomedical Circuits and Systems* **2014**, *8*, 177–185.

(21) Rothberg, J. M.; Hinz, W.; Rearick, T. M.; Schultz, J.; Mileski, W.; Davey, M.; Leamon, K., John H.and Johnson; Milgrew, M. J.; Edwards, M.; et al., An integrated semiconductor device enabling non-optical genome sequencing. *Nature* **2011**, *475*, 348 – 352.

(22) Kinlen, P.; Frushour, B.; Ding, Y.; Menon, V. International Conference on Science and Technology of Synthetic Synthesis and Characterization of Organically Soluble Polyaniline and Polyaniline Block Copolymers. *Synthetic Metals* **1999**, *101*, 758 – 761.

(23) Georgiou, P.; Toumazou, C. ISFET characteristics in CMOS and their application to weak inversion operation. *Sensors and Actuators B: Chemical* **2009**, *143*, 211 – 217.

(24) Bobacka, J.; Ivaska, A.; Lewenstam, A. Potentiometric Ion Sensors. *Chemical Reviews* **2008**, *108*, 329–351.

(25) Hu, J.; Stein, A.; Buhlmann, P. Rational design of all-solid-state ion-selective electrodes and reference electrodes. *TrAC Trends in Analytical Chemistry* **2016**, *76*, 102 – 114.

(26) van de Velde, L.; d'Angremont, E.; Olthuis, W. Solid contact potassium selective electrodes for biomedical applications - a review. *Talanta* **2016**, *160*, 56 – 65.

(27) He, N.; Gyurcsanyi, R. E.; Lindfors, T. Electropolymerized hydrophobic polyazulene as solid-contacts in potassium-selective electrodes. *Analyst* **2016**, *141*, 2990–2997.

(28) Boeva, Z. A.; Lindfors, T. Few-layer graphene and polyaniline composite as ion-to-electron transducer in silicone rubber solid-contact ion-selective electrodes. *Sensors and Actuators B: Chemical* **2016**, *224*, 624 – 631.

(29) Buck, R. a. L. Recommendations for nomenclature of ionselective electrodes (IUPAC Recommendations 1994). *Pure and Applied Chemistry* **2012**, 2527–2536.

(30) Lewenstam, A. Routines and Challenges in Clinical Application of Electrochemical Ion-Sensors. *Electroanalysis* **2014**, *26*, 1171–1181.

(31) Dillingham, P. W.; Radu, T.; Diamond, D.; Radu, A.; McGraw, C. M. Bayesian Methods for Ion Selective Electrodes. *Electroanalysis* **2012**, *24*, 316–324.

(32) Kamahori, M.; Ishige, Y.; Shimoda, M. Detection of DNA hybridization and extension reactions by an extended-gate field-effect transistor: Characterizations of immobilized DNA probes and role of applying a superimposed high-frequency voltage onto a reference electrode. *Biosensors and Bioelectronics* **2008**, *23*, 1046 – 1054.

(33) Fixe, F.; Branz, H.; Louro, N.; Chu, V.; Prazeres, D.; Cond, J. Immobilization and hybridization by single sub-millisecond electric field pulses, for pixel-addressed DNA microarrays. *Biosensors and Bioelectronics* **2004**, *19*, 1591 – 1597.

(34) Kaisti, M.; Zhang, Q.; Prabhu, A.; Lehmusvuori, A.; Rahman, A.; Levon, K. An Ion-Sensitive Floating Gate FET Model: Operating Principles and Electrofluidic Gating. *IEEE Transactions on Electron Devices* **2015**, *62*, 2628–2635.

Graphical TOC Entry